Applied Physics A (2020) 126:717
https://doi.org/10.1007/s00339-020-03918-3

Applied Physics A
Materials Science & Processing

Reflective photonic nanojets generated from cylindrical concave micro-mirrors

Wen Yang[1] · Rong Gao[1] · Yimin Wang[1] · Song Zhou[1] · Juchen Zhang[1]

Received: 12 June 2020 / Accepted: 13 August 2020

Abstract

Reflective photonic nanojets (r-PNJs) produced by cylindrical concave micro-mirrors are numerically investigated. Simulation shows that the full-width at half-maximum (FWHM) of the r-PNJ is associated with the angle of the cylindrical concave mirror. It is found that the FWHM of the r-PNJ can achieve 0.37 of the wavelength, when the mirror with the angle $\theta = 130°$ is put in air. For the concave mirror immersed in water with $\theta = 100°$, the FWHM of the r-PNJ can reach about 0.3λ. Two symmetric vortexes of Poynting vectors are close to the r-PNJ, which leads to the narrowed r-PNJ. Through combining a dielectric micro-cylinder with the concave mirror immersed in water, the waist of the r-PNJ can achieve 0.27 of the incident wavelength.

Keywords Photonic nanojets · Reflection mode · Concave mirror

1 Introduction

It is known that both lenses and concave mirrors can converge light to the focal spot [1]. Lenses adopt the transmission mode, while concave mirrors utilize the reflection mode. However, the limit imposed by the diffraction of optical waves restricts generation of sub-wavelength focal spots [2]. The capability of generating photonic nanojets (PNJs) that allows overcoming the diffraction limited resolution [3–5] has been proposed and demonstrated experimentally using microspheres [6–9] and micro-cylinders [10–12]. PNJs formed by microspheres and micro-cylinders illuminated under a plane wave are distributed at the shadow of the micro-particles. These PNJs are produced in transmission mode.

Focusing of a dielectric particle on a silicon substrate with a nano-gap was investigated in [13]. However, the calculation of the intensity distribution inside the sphere was not mentioned. Later, PNJs generated in reflection mode with wide-angle performance were produced by hemispherical particles on metallic substrates in [14] and three-dimensional dielectric cuboids on metallic substrates in [15–17], demonstrating the capability to make r-PNJs localized out of the particles. Recently, it was experimentally found that a thin rectangular dielectric–metal structure could have a function of a flat focusing mirror based on photonic jet effect in reflection mode in [18]. In [19], a new method to produce r-PNJs using high refractive index contrast between a near-unity-index microsphere lens and a high-index dielectric substrate was successfully produced. The FWHM of the r-PNJ could reach 0.48 of wavelength, which localizes out of the microsphere. A specific regime of near-field focusing, called *s*-PNJ, supported by a dielectric micro-cylinder located near a metal mirror was presented in [20]. In [21], the detailed physical basis of the *s*-PNJs was reported.

Several years ago, spherical and cylindrical concave micro-mirrors utilizing silicon were fabricated in [22, 23]. In [24], silicon spherical and cylindrical micro-mirrors enabled lensless efficient coupling of free light. The microscale concave surfaces used for displaying colorful iridescence in reflection were reported in [25]. Recently, reflective photonic hook was achieved by dielectric coated concave hemi-cylindrical mirror in [26]. Herein, we investigated the cylindrical concave micro-mirror for the r-PNJ generation. At first, we investigate the influence of the angle of the cylindrical concave mirror on the properties of the r-PNJs. It is found that the FWHM of the r-PNJ can achieve less than half of the

✉ Song Zhou
zs41080218@126.com

[1] Jiangsu Key Laboratory of Advanced Manufacturing Technology, Faculty of Mechanical and Material Engineering, Huaiyin Institute of Technology, Huai'an 223003, China

Published online: 19 August 2020

incident wavelength. Then, the concave micro-mirror which is immersed in water for the improvement of the FWHM of the r-PNJ is presented. Poynting vectors close to the r-PNJs are also studied. It is showed that the waist of the r-PNJ reaches approximately λ/3, and two symmetric vortexes of Poynting vectors are close to the r-PNJs. The narrower r-PNJ can be obtained by putting a micro-cylinder on the concave micro-mirror. Finally, the deformation of the mirror surface is adopted to show the influences of the manufacturing accuracy of the mirror surface on the r-PNJs.

2 Models and methods

To investigate the r-PNJs' performance, a 2D full-wave computation utilizing the COMSOL Multiphysics finite element method-based commercial software package [27] is implemented. The schematic diagram of the model is shown in Fig. 1. The angle of the cylindrical concave mirror with $H = 4$ μm, $L = 8$ μm, and $R = 3$ μm is defined as θ. In our simulation, the incident TE-polarization plane wave, with a wavelength of $\lambda = 638$ nm and $E_0 = 1$, is added as a background field into the software package. Perfectly matched layer absorbing boundary conditions are utilized around the computational domain. Light intensity is defined as the full electric field squared. To guarantee the accuracy of the simulation, the maximum element size of the free triangular mesh is set to 20 nm in the computational domain. Gold medium is employed at the concave mirror to reflect the incident wave.

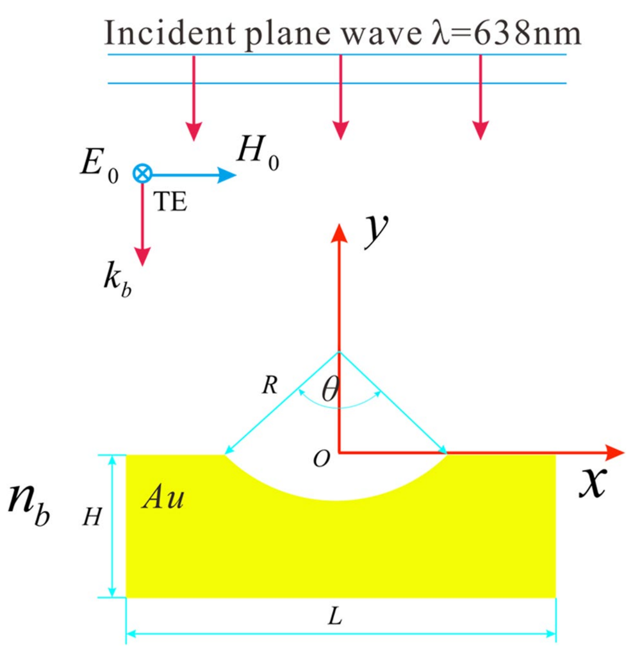

Fig. 1 Schematic diagram of the model: a gold cylindrical concave micro-mirror illuminated by a TE-polarization plane wave

For the considered wavelength, the dielectric permittivity of gold is selected from [28, 29] as $\varepsilon_{\mathrm{Au}} = -12.241 + 1.2048i$. The gold concave micro-mirror is put in a medium with the refractive index $n_b = 1$.

3 Results and discussions

First, focusing performance of the r-PNJ is evaluated by changing the angle θ of the cylindrical concave mirror shown in Fig. 1. Numerical results of the intensity distributions of the r-PNJs for angle θ ranging from 90° to 150° with a step of 10° are shown in Fig. 2. It is observed that patterns of the r-PNJs are different from that presented in [19]. As can be seen in Fig. 2a, the focal pattern is divided into two segments, while the intensity of upper pattern is larger than the lower one. With the increasing of the angle θ, intensity of the lower pattern becomes larger than that of the upper one, as shown in Fig. 2b and c. From the simulation results shown in Fig. 2d, it is indicated that the intensity of the r-PNJs can be maximized when the angle is chosen as $\theta = 130°$. The FWHMs of the focal spots are less than 319 nm (~ $\lambda/2$), as shown in Fig. 2d. In Fig. 3, intensity distributions of the r-PNJs generated by a gold concave mirror and an ideal perfect-reflection mirror with the radian $\theta = 130°$ are displayed. Comparing intensity distributions between them, the r-PNJs formed by the ideal perfect-reflection mirror are similar to the gold mirror. The maximum intensity of r-PNJ formed by the gold mirror is less than that produced by an ideal perfect-reflection mirror, as can be seen in Fig. 3c. The FWHMs of the r-PNJs generated by these two types of mirror are close to 237.2 nm (~ 0.37λ).

Then, r-PNJs formed by the concave mirror immersed in water are investigated. Focusing performance of the r-PNJ is studied by changing the angle θ ranged from 90° to 150° with a step of 10°. It is showed that the maximum intensity appears when the angle is selected as $\theta = 100°$ in the simulation. Intensity distribution of the r-PNJ produced by the concave mirror at the angle $\theta = 100°$ is shown in Fig. 4a. Meanwhile, the intensity distribution along x-axis at the focal plane is shown in Fig. 4b. In comparison of the maximum intensity of the r-PNJ formed by the concave mirror with $\theta = 130°$ put in air and the mirror with $\theta = 100°$ immersed in water, it is found that the maximum intensity of the r-PNJ can be improved with the mirror immersed in water and its waist is 191.2 nm (about 0.3λ), which is narrower than that shown in Fig. 3a. The FWHM reaches 0.3λ less than $\lambda/2n_b$ (where n_b is selected as 1.33). Thus, the reflective focusing approach beats the diffraction limit through utilizing the gold cylindrical concave micro-mirrors. To investigate the mechanism of diffraction limit broken with this concave mirror, distribution of P_y (y-component of the Poynting vector) of the r-PNJs formed by the concave mirror and

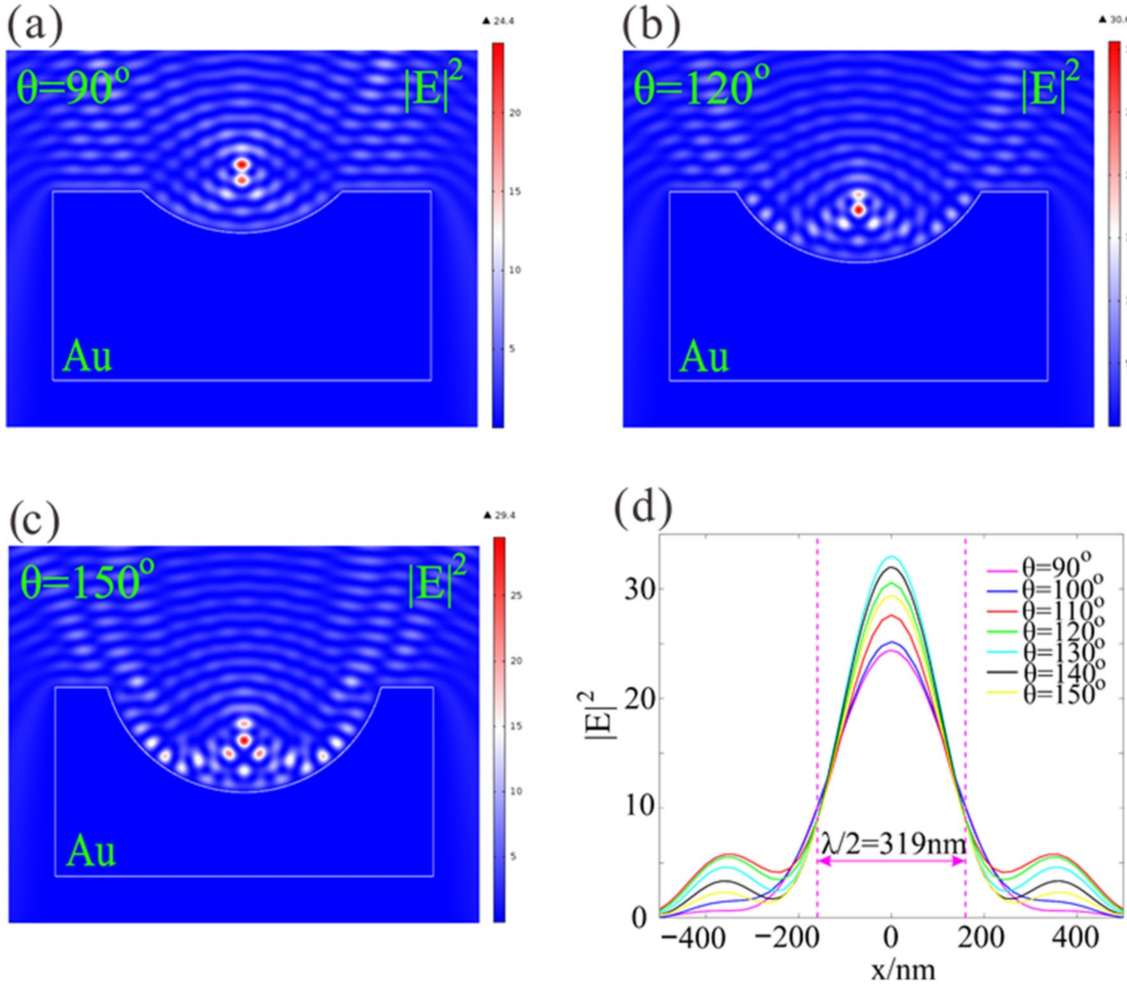

Fig. 2 Reflective photonic nanojets formed by the cylindrical concave mirrors with different radians. Intensity distributions of the reflected photonic nanojets produced by the mirror with the radian $\theta = 90°$ in (**a**), $\theta = 120°$ in (**b**) and $\theta = 150°$ in (**c**). Intensity distributions along x-axis at the focal planes for the radians ranging from 90° to 150° with a step of 10° in (**d**)

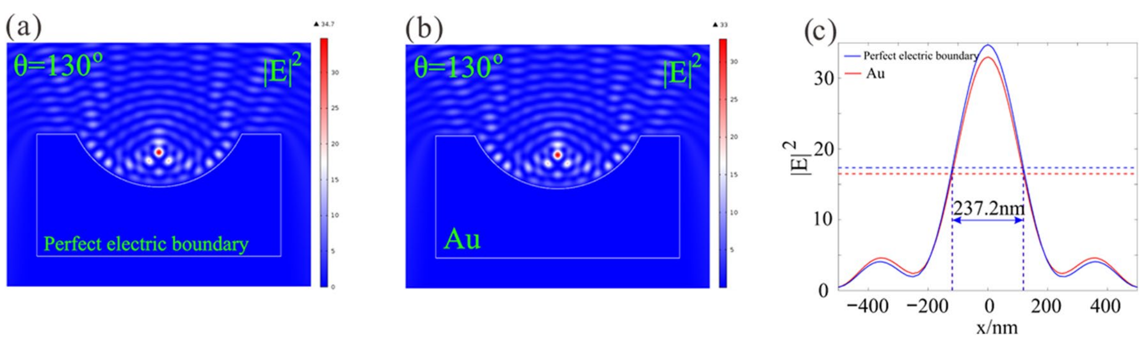

Fig. 3 Reflective photonic nanojets formed by the cylindrical concave mirrors with the radian $\theta = 130°$. Intensity distributions of the reflective photonic nanojets produced by the ideal perfect-reflection mirror in (**a**) and the gold mirror in (**b**). Intensity distributions along x-axis at the focal planes for these two kinds of mirrors in (**c**)

the Poynting vectors close to the r-PNJs are calculated. The results are shown in Fig. 4c and 4d. The value of P_y of the concave mirror immersed in water with $\theta = 100°$ is larger than that shown in Fig. 3a. The distribution of P_y is consistent with intensity distribution. From the insert figures shown in Fig. 4c and d, it is indicated that two symmetric

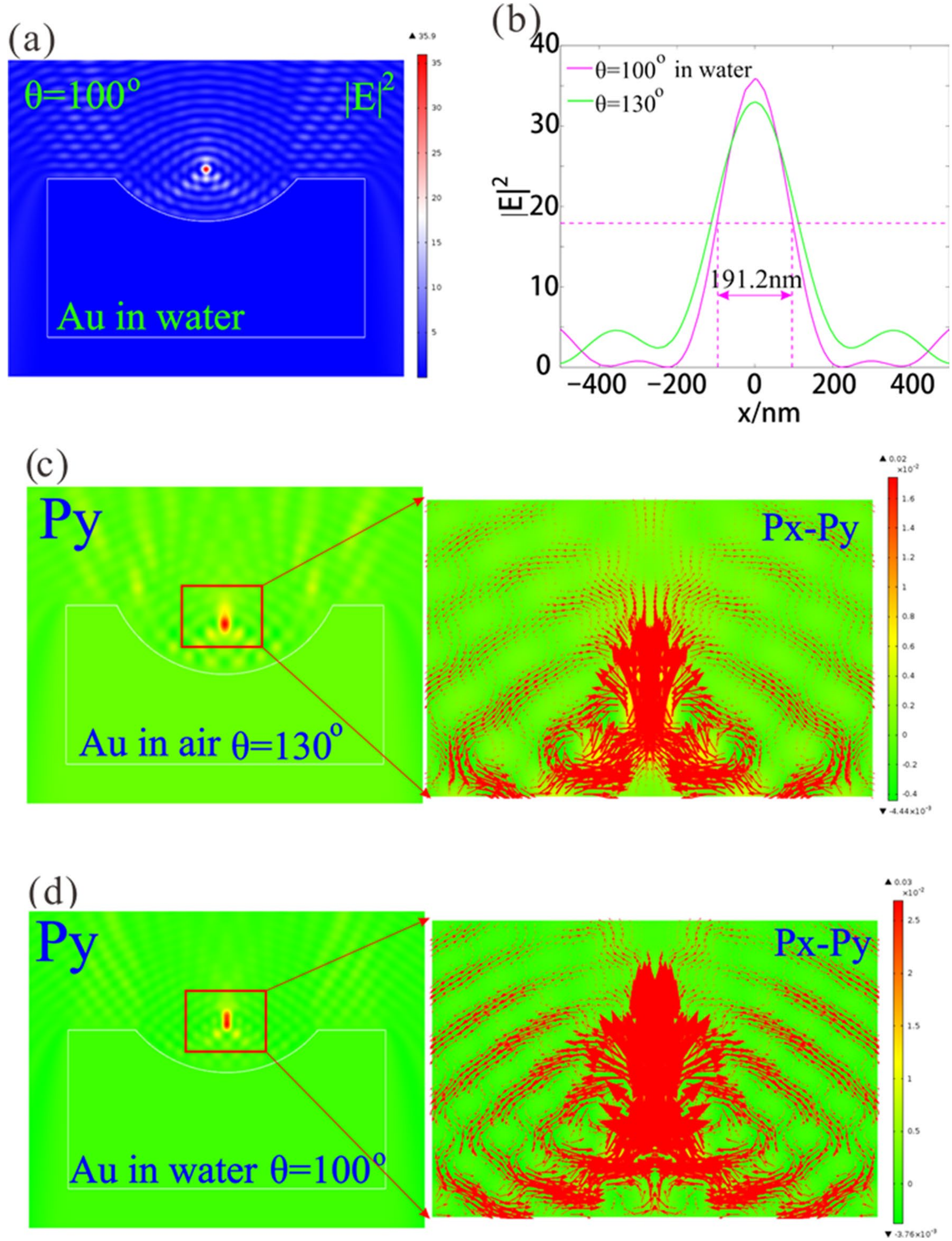

Fig. 4 **a** Reflective photonic nanojet formed by the cylindrical concave mirror with the radian $\theta = 100°$ immersed in water. **b** Intensity distribution along x-axis at the focal plane for the mirror with the radian $\theta = 100°$ immersed in water, the mirror with the radian $\theta = 130°$ put in air as a reference. **c** Distribution of P_y (y-component of the Poynting vector) of the reflective photonic nanojet formed by the mirror with the radian $\theta = 130°$ put in air, insert figure: the Poynting vectors close to the r-PNJ. **d** Distribution of P_y of the reflective photonic nanojet shown in (**a**), insert figure: the Poynting vectors close to the r-PNJ

vortexes of Poynting vectors are distributed near the r-PNJs. It is known that power flows normally couple to the other planes through the singularities in these vortexes [30]. This causes high-intensity region at the center line of the r-PNJ and makes narrower beam waist. In [31], it was reported that the formation of optical vortices can lead to high light localization and the FWHM of beam waist less than the diffraction limit given by $\lambda/2n$ was related to superoscillations [32]. On the other side, the supercritical lens can produce less than diffraction limit spots without obvious side lobes [33]. The physical basis for the r-PNJ without side lobes shown in Fig. 4a may be similar to the high light localization shown in [31].

The structure with a micro-cylinder put on the concave mirror is investigated. The diameter of the micro-cylinder is selected as 1 µm, and its refractive index is $n_c = 1.46$. Moreover, the cylinder lens and the concave mirror are both immersed in water. The computation results are presented in Fig. 5. From Fig. 5a and c, it is indicated that the intensity of the r-PNJ is distributed out of the micro-cylinder. With the assistance of the concave mirror, the FWHM reaches 173 nm (about 0.27λ). At the focal plane, the FWHM of normalized $|P_y|$ is less than 0.27λ. To investigate the physics of those results in Fig. 5, three kinds of Gaussian beam illuminations are adopted. The results are shown in Fig. 6. In Fig. 6a, the Gaussian beam illumination with the beam width d represents the main light which propagates twice through the cylinder. Intensity distribution shown in the left of Fig. 6a is similar to that of the r-PNJ formed by a cylinder on the flat mirror shown in Fig. 1d in [20]. The difference of r-PNJs formed by a cylinder on the concave mirror and the flat mirror is that partial light without propagating through the cylinder before reflected by the concave mirror can be collected by the cylinder at the assistant of the reflection of the concave mirror. This process is illustrated in Fig. 6b. In Fig. 6c, the intensity distribution is close to that shown in

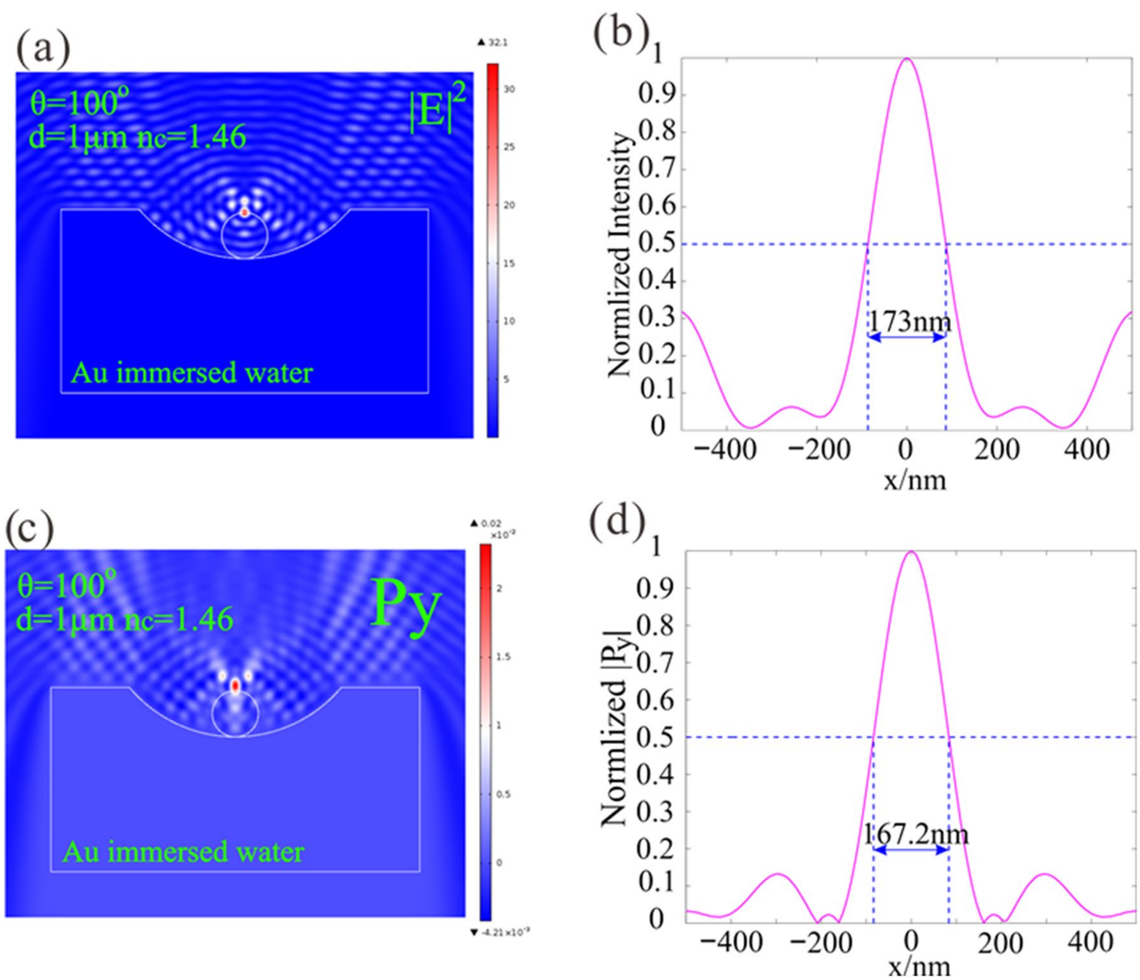

Fig. 5 **a** Reflective photonic nanojet formed by the cylindrical concave mirror with the radian $\theta = 100°$ and a micro-cylinder with diameter 1 um and refractive index $n_c = 1.46$ immersed in water. **b** Normalized intensity distribution along x-axis at the focal plane for the structure shown in (**a**). **c** Distribution of P_y (y-component of the Poynting vector) of the concave mirror and the cylinder lens. **d** Normalized $|P_y|$ along x-axis at the focal plane for the reflected photonic nanojet shown in (**a**)

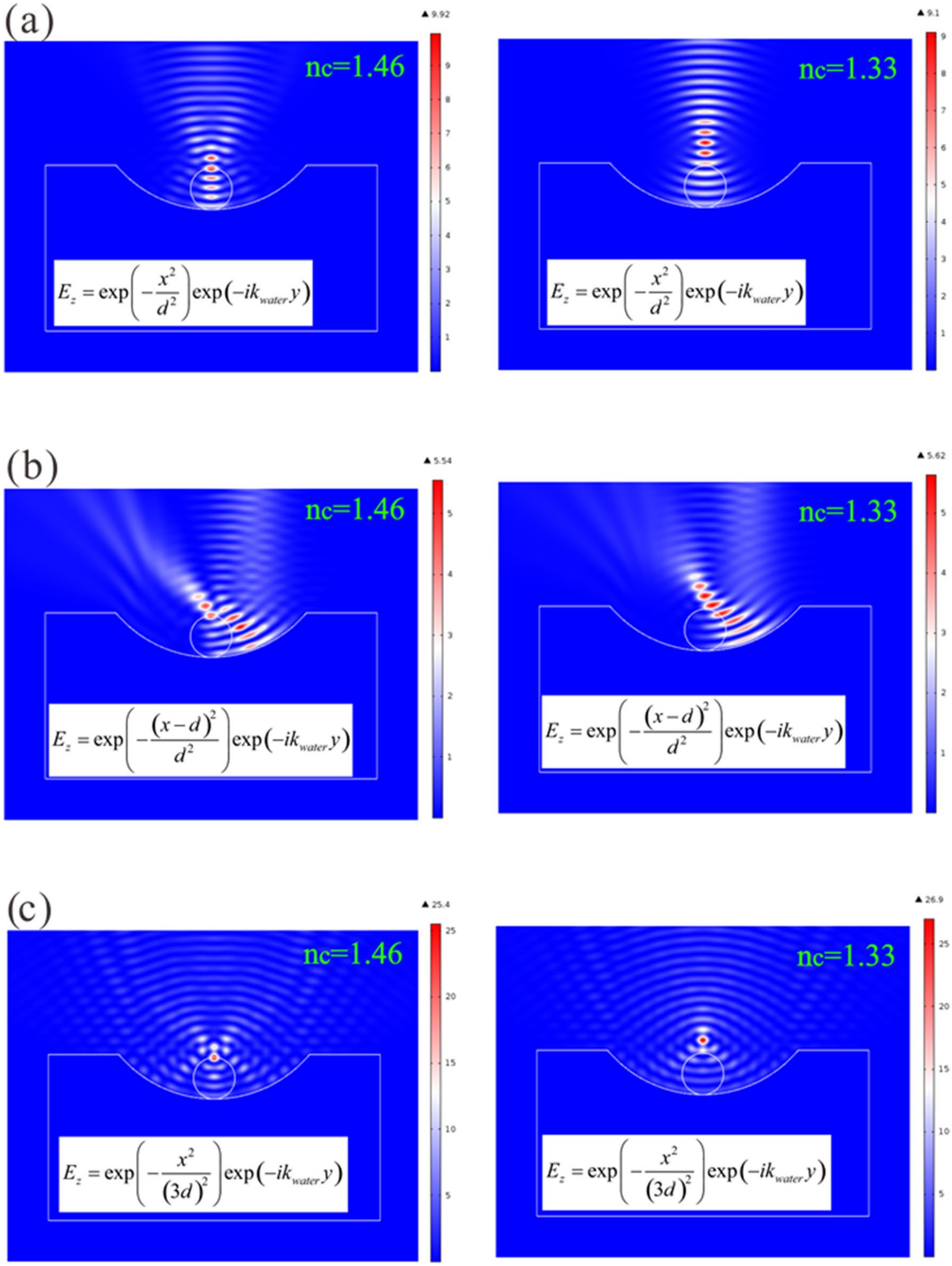

Fig. 6 Intensity distributions of the concave mirror with and without a cylinder illuminated under the Gaussian beam with beam width d in (**a**) and (**b**), and $3d$ in (**c**). The center offset of the Gaussian beam is d in (**b**), and all the other parameters are selected the same with those in Fig. 5

Fig. 5a by increasing the Gaussian beam width. In comparison with the structure without using a cylinder, it can be seen that the focal planes of the concave mirror with a cylinder are closer to the concave surface. The employment of cylinder on the concave mirror causes optical path difference and changes the focal position and properties of the r-PNJ.

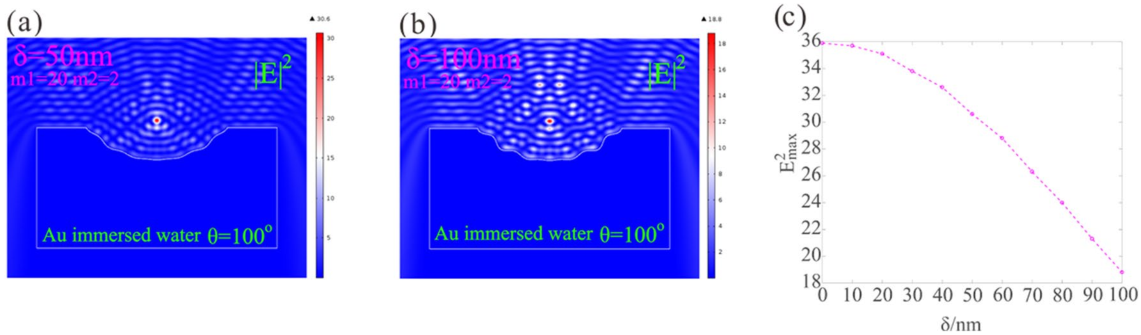

Fig. 7 Reflective photonic nanojet formed by the rough concave mirror with $\delta = 50$ nm in (**a**), and $\delta = 100$ nm in (**b**). **c** The maximum intensity of the reflective photonic nanojet as the function of the the deformation δ. The parameters are selected as $R = 3$ µm, $m_1 = 20$, and $m_2 = 2$

In [21], the effect of the surface roughness of a reflecting mirror on the maximum intensity of the r-PNJ was presented. For the circular surface, the deformation at its boundary can be used to show the effect of rough surface on the PNJs formation in [34]. Herein, we use the method described in [34] to show the influence of the manufacturing accuracy of the mirror surface on the r-PNJs. The radius of the concave mirror can be expressed as $R(\varphi) = R + \delta\ \sin(m_1\varphi)\sin(m_2\varphi)$, where R is the average radius of the concave mirror, δ is the deformation of the concave surface to the average radius, m_1 and m_2 are the two periods of the variations of the corrugated boundary with φ being the azimuth angle. In the simulation, $R = 3$ µm, $m_1 = 20$ and $m_2 = 2$ are selected and the structure shown in Fig. 4a is employed. The results are shown in Fig. 7. It can be seen that the increase in the roughness of the concave surface leads to worsening r-PNJ distribution and is expressed in decrease in its intensity and in stray light intensifies. For the deformation $\delta = 50$ nm, there is a ~ 15% decrease of r-PNJ maximum intensity in comparison with the smooth surface. From the results in Fig. 7, it is indicated that the r-PNJ is slightly changed if the deformation δ is less than 50 nm.

4 Conclusion

In conclusion, the capability to generate r-PNJs utilizing a cylindrical concave micro-mirror working in the reflection mode has been investigated. It is found that the FWHM of the r-PNJ can achieve 0.37 of the wavelength, when the mirror with the angle $\theta = 130°$ is put in air. For the concave mirror with $\theta = 100°$ immersed in water, the FWHM of the r-PNJ is decreased to about 0.3λ. Moreover, two symmetric vortexes of Poynting vectors distributed close to the r-PNJs are presented. This may be the mechanism for diffraction limit broken focusing through utilizing this concave mirror. The waist of the r-PNJ can achieve 0.27λ by putting a micro-cylinder on the concave mirror with the angle $\theta = 100°$ immersed in water. Finally, simulation shows that surface roughness ($\delta \geq 50$ nm) of the concave mirror can degrade r-PNJ distribution and stray light intensifies. This result may be of interest for super-resolution optical microscopy in reflection mode, such as imaging biomedical particles in liquid, which is situated at the top of the cylinder.

Acknowledgements This work was supported by the open fund HGAMTL-1803 from Jiangsu Key Laboratory of Advanced Manufacturing Technology.

Compliance with ethical standards

Conflict of interest The authors declare no conflicts of interest.

References

1. F.A. Jenkins, H.E. White, *Fundamentals of optics* (Tata McGraw-Hill Education, New York, 1937)
2. M. Born, E. Wolf, *Principles of optics: electromagnetic theory of propagation, interference and diffraction of light* (Elsevier, Amsterdam, 2013)
3. A. Heifetz, S.C. Kong, A.V. Sahakian, A. Taflove, V. Backman, Photonic nanojets. J. Comput. Theor. Nanosci. **6**(9), 1979–1992 (2009)
4. B.S. Luk'yanchuk, R. Paniagua-Domínguez, I.V. Minin, O.V. Minin, Z. Wang, Refractive index less than two: photonic nanojets yesterday, today and tomorrow. Opt. Mater. Express **7**(6), 1820–1847 (2017)
5. J. Zhu, L.L. Goddard, All-dielectric concentration of electromagnetic fields at the nanoscale: the role of photonic nanojets. Nanoscale Adv. **1**(12), 4615–4643 (2019)
6. Z. Chen, A. Taflove, V. Backman, Photonic nanojet enhancement of backscattering of light by nanoparticles: a potential novel visible-light ultramicroscopy technique. Opt. Express **12**(7), 1214–1220 (2004)
7. Z. Wang, W. Guo, L. Li, B.S. Luk'yanchuk, A. Khan, Z. Liu, Z. Chen, M. Hong, Optical virtual imaging at 50 nm lateral resolution with a white-light nanoscope. Nat. Commun. **2**(1), 1–6 (2011)
8. H. Yang, R. Trouillon, G. Huszka, A.M.M. Gijs, Super-resolution imaging of a dielectric microsphere is governed by the waist of its photonic nanojet. Nano Lett. **16**(8), 4862–4870 (2016)

9. L. Chen, Y. Zhou, Y. Li, M. Hong, Microsphere enhanced optical imaging and patterning: from physics to applications. Appl. Phys. Rev. **6**(2), 021304 (2019)
10. C.-Y. Liu, K.L. Hsiao, Direct imaging of optimal photonic nanojets from core-shell microcylinders. Opt. Lett. **40**(22), 5303–5306 (2015)
11. A. Darafsheh, D. Bollinger, Systematic study of the characteristics of the photonic nanojets formed by dielectric microcylinders. Opt. Commun. **402**, 270–275 (2017)
12. J.N. Monks, B. Yan, N. Hawkins, F. Vollrath, Z. Wang, Spider silk: mother nature's bio-superlens. Nano Lett. **16**(9), 5842–5845 (2016)
13. B.S. Luk'Yanchuk, Z. Wang, W. Song, M. Hong, Particle on surface: 3D-effects in dry laser cleaning. Appl. Phys. A **79**(4), 747–751 (2004)
14. I.V. Minin, O.V. Minin, N.A. Kharitoshin, Localized high field enhancements from hemispherical 3D mesoscale dielectric particles in the refection mode. In: *2015 16th International Conference of Young Specialists on Micro/Nanotechnologies and Electron Devices, EDM 2015—Proceedings*
15. I.V. Minin, O.V. Minin, V. Pacheco-Peña, M. Beruete, Localized photonic jets from flat, three-dimensional dielectric cuboids in the reflection mode. Opt. Lett. **40**(10), 2329–2332 (2015)
16. I.V. Minin, O.V. Minin, I.S. Nefedov, Photonic jets from Babinet's cuboid structures in the reflection mode. Opt. Lett. **41**(4), 785–787 (2016)
17. I.V. Minin, O.V. Minin, V. Pacheco-Peña, M. Beruete, Subwavelength, standing-wave optical trap based on photonic jets. Quantum Electron. **46**(6), 555 (2016)
18. I.V. Minin, C.-Y. Liu, Y.-C. Yang, K. Staliunas, O.V. Minin, Experimental observation of flat focusing mirror based on photonic jet effect. Sci. Rep. **10**(1), 8459 (2020)
19. L. Yue, B. Yan, J.N. Monks, R. Dhama, Z. Wang, O.V. Minin, I.V. Minin, Photonic jet by a near-unity-refractive-index sphere on a dielectric substrate with high index contrast. Ann. Phys. **530**(6), 1800032 (2018)
20. Y.E. Geints, A.A. Zemlyanov, I.V. Minin, O.V. Minin, Overcoming refractive index limit of mesoscale light focusing by means of specular-reflection photonic nanojet. Opt. Lett. **45**(14), 3885–3888 (2020)
21. I.V. Minin, Y. Geints, A. Zemlyanov, O.V. Minin, An extensive study of specular-reflection photonic nanojet: Physical basis and optical trapping application. Opt. Express **28**(15), 222690–222704 (2020)
22. Y.S. Ow, M.B.H. Breese, S. Azimi, Fabrication of concave silicon micro-mirrors. Opt. Express **18**(14), 14511–14518 (2010)
23. Y. Bao, F. Zhou, T.W. LeBrun, J.J. Gorman, Concave silicon micromirrors for stable hemispherical optical microcavities. Opt. Express **25**(13), 15493–15503 (2017)
24. Y. Sabry, B. Saadany, D. Khalil, T. Bourouina, Silicon micromirrors with three-dimensional curvature enabling lensless efficient coupling of free-space light. Light Sci. Appl. **2**, e94 (2013)
25. A.E. Goodling, S. Nagelberg, B. Kaehr, C.H. Meredith, S.I. Cheon, A.P. Saunders, M. Kolle, L.D. Zarzar, Colouration by total internal reflection and interference at microscale concave interfaces. Nature **566**(7745), 523–527 (2019)
26. C.Y. Liu, H.J. Chung, E. Hsuan-Pei, Reflective photonic hook achieved by dielectric-coated concave hemi-cylindrical mirror. J. Opt. Soc. Am. B Opt. Phys. **37**, 2528–2533 (2020). https://doi.org/10.1364/JOSAB.399434
27. https://cn.comsol.com/. Accessed 18 Aug 2020
28. P.B. Johnson, R.W. Christy, Optical constants of the noble metals. Phys. Rev. B **6**(12), 4370 (1972)
29. A.D. Rakić, A.B. Djurišić, J.M. Elazar, M.L. Majewski, Optical properties of metallic films for vertical-cavity optoelectronic devices. Appl. Opt. **37**(22), 5271–5283 (1998)
30. Z. Wang, B.S. Luk'Yanchuk, M. Hong, Y. Lin, T. Chong, Energy flow around a small particle investigated by classical Mie theory. Phys. Rev. B **70**(3), 035418 (2004)
31. Z. Wang, B.S. Lu'kyanchuk, L. Yue, B. Yan, J. Monks, R. Dhama, O.V. Minin, I.V. Minin, S. Huang, A.A. Fedyanin, High order Fano resonances and giant magnetic fields in dielectric microspheres. Sci. Rep. **9**(1), 20293 (2019)
32. K. Huang, H. Ye, J. Teng, S.P. Yeo, B.S. Luk'yanchuk, C.-W. Qiu, Optimization-free superoscillatory lens using phase and amplitude masks. Laser Photonics Rev. **8**(1), 152–157 (2014)
33. F. Qin, K. Huang, J. Wu, J. Teng, C.-W. Qiu, M. Hong, A supercritical lens optical label-free microscopy: sub-diffraction resolution and ultra-long working distance. Adv. Mater. **29**(8), 1602721 (2017)
34. I. Mathariq, V.N. Astratov, H. Kurt, Persistence of photonic nanojet formation under the deformation of circular boundary. J. Opt. Soc. Am. B **33**(4), 535 (2016)